# JuSPARC — The Jülich Short-Pulsed Particle and Radiation Center

Forschungszentrum Jülich, Peter Grünberg Institute (PGI-6) [*]

Scientists:
- Dr. Roman Adam, PGI-6, phone: +49 2461 61 5196, email: r.adam@fz-juelich.de
- Dr. Christian Tusche, PGI-6, phone: +49 2461 61 4627, email: c.tusche@fz-juelich.de
- M.Sc. Anna Hützen, PGI-6, phone: +49 2461 61 3485, email: a.huetzen@fz-juelich.de
- Dr. Carsten Wiemann, PGI-6, phone: +49 2461 61 1486, email: c.wiemann@fz-juelich.de
- Dr. Ying-Jiun Chen, PGI-6, phone: +49 2461 61 1486, email: yi.chen@fz-juelich.de
Management:
- Prof. Dr. Markus Büscher, PGI-6, phone: +49 2461 61 6669, email: m.buescher@fz-juelich.de
- Prof. Dr. Claus M. Schneider, PGI-6, phone: +49 2461 61 4428, email: c.m.schneider@fz-juelich.de

**Abstract:** *Ju*SPARC, the Jülich Short-Pulsed Particle and Radiation Center, is a laser-driven facility to enable research with short-pulsed photon and particle beams to be performed at the Forschungszentrum Jülich. The conceptual design of *Ju*SPARC is determined by a set of state-of-the-art time-resolved instruments, which are designed to address the electronic, spin, and structural states of matter and their dynamic behaviour. From these instruments and experiments *Ju*SPARC derives the need of operating several dedicated high pulse-power laser systems at highest possible repetition rates. They serve as core units for optimized photon up-conversion techniques generating the light pulses for the respective experiments. The applications also include experiments with spin-polarized particle beams, which require the use of laser-based polarized gas targets. Thus, in its first stage *Ju*SPARC comprises four driving laser systems, called *Ju*SPARC_VEGA, *Ju*SPARC_DENEB, *Ju*SPARC_SIRIUS and *Ju*SPARC_MIRA, which are outlined in this article.

## 1 Introduction

A major challenge common to many different scientific fields is the in-depth understanding and subsequent control of dynamic and non-equilibrium processes on short time scales ranging down into the femto- and attosecond regime. Examples are electronic, magnetic and structural phase transitions in condensed matter physics and materials science, energy and angular momentum transfer processes in

information technology and energy science, or reaction kinetics and dynamics in chemistry, biology and even medicine. These processes may be driven by a variety of external stimuli, involving temperature, pressure, electromagnetic fields, charge or spin currents. As a complication many technologically relevant processes often involve several subsequent steps taking place on hierarchical time scales. This situation asks for dedicated and highly specialized experimental and theoretical approaches to disentangle the relevant microscopic mechanisms and to follow their temporal evolution.

The progress in Information Technology follows the trends *smaller — faster — cooler*, the latter trend describing the need to reduce the energy consumption of nanoelectronic devices. Energy efficiency is also a strong driver for exploring alternative concepts to store and manipulate information. Among others, these include the use of the electron spin, redox ions, or structural phase transitions. The control of the electron spin offers widespread applications ranging from spintronics (information storage and processing) to quantum computing (Tsymbal & Zutic, 2012), whereas the latter concepts promise applications in low-power nonvolatile memory and neuromorphic computing (Ielmini & Waser, 2016). As a specific example, the controlled manipulation of electron spin ensembles and spin currents on ultra-short time scales is at the heart of magnetic data storage and spintronics. Current research addresses among others issues such as all-optical magnetic switching, ultrafast demagnetization phenomena, super-diffusive spin currents, magnetic phase transitions, metal-insulator transitions, or coupled spin-charge-orbital ordering phenomena. On a more microscopic level these phenomena translate into a complex interplay of quantum-mechanical interactions involving different length and energy scales (Figure 1).
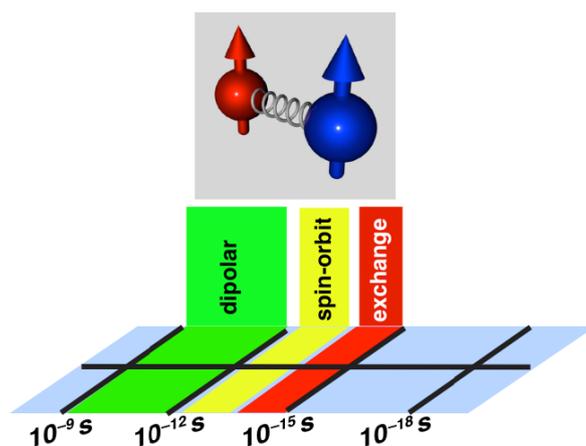


Figure 1: Fundamental interactions and relevant time scales in magnetism and spintronics.

In particular, these energy scales can be related to characteristic time scales on which processes take place. The strongest interaction in spin-based systems is the exchange interaction involving an energy scale of eV. Exchange-driven processes thus involve typical time scales of $\sim 10\,\text{fs}$, whereas electronic excitations, *e.g.* from core levels may reach into the sub-fs regime. Taking into account the richness of material systems in spintronics, experiments aiming to investigate the impact of these interactions must combine element specificity and spin sensitivity with a very high time resolution. Similar considerations hold for the other areas in information technology, where electronic phase transitions, local electrochemical processes or recrystallization/amorphization processes in phase change materials are involved, as electronic time scales also reach into the sub-femtosecond regime. Photons provide the most versatile basis for characterization, as they are able to probe structural, electronic, and spin aspects, individually and in combination. This situation calls for highly specialized photon sources providing ultrashort pulses.

## 2   The *Ju*SPARC Concept

Experimentally, the scientific challenges discussed above should and could be addressed by a broad portfolio of state-of-the-art characterization techniques employing short and ultrashort photon pulses of wavelength and polarization state appropriately chosen for the individual question. *Ju*SPARC plans for following techniques and photon energy ranges:

A. *Photon-in/Electron-out* – These approaches address mainly the time-dependent electronic band structure in condensed matter systems and include angle-resolved photoemission spectroscopy (ARUPS) and momentum microscopy. Particular emphasis is laid on the explicit analysis of the photoelectron spin. The required photon energies range from $[\sim \mathbf{10}, \sim \mathbf{150}]$ eV (XUV).

B. *Photon-in/Photon-out* – These approaches encompass time-resolved soft x-ray absorption spectroscopy (XAS) and their variants. Employing the photon energy range from $[\sim \mathbf{100}, \sim \mathbf{1200}]$ eV (soft x-ray) provides access to characteristic core levels of most relevant elements, which is the basis for chemical specificity. The polarization state of the light (circular, linear) can be exploited to disentangle magnetic states, orbital and spin ordering phenomena, as well as dichroisms of various nature.

C. *Photon-in/Photon-out* – Photon energies in the range of $[\sim \mathbf{0.5}, \sim \mathbf{10}]$ keV (tender or hard x-ray) enable access to structural parameters and their temporal evolution via a suite of time-resolved x-ray scattering experiments.

The general nature of scattering, spectroscopy or microscopy investigations with high time resolution involves advanced pump-probe schemes: the system under study is excited by a pulsed stimulus, thereby creating a transient state, the temporal evolution of which is mapped by a time-delayed probe pulse. An important ingredient to obtain ultimate time resolution is a stable and controlled delay between pump and probe pulses. The development of the respective experimental approaches is thus closely connected to the advent of appropriate short-pulse sources of photons, electrons or neutrons. In many experiments the most prominent combination of pump and probe pulses involves photons. Access to soft x-ray pulses in the femtosecond regime, however, requires either specific bunch slicing procedures or free electron lasers. In these approaches the presently achievable time-resolution is of the order of a few 10 fs. From the scientific challenges described above the need for a novel type of table-top laser-based experimental facilities, such as *Ju*SPARC has been derived, which establish a third pillar in the photon landscape (Figure 2).
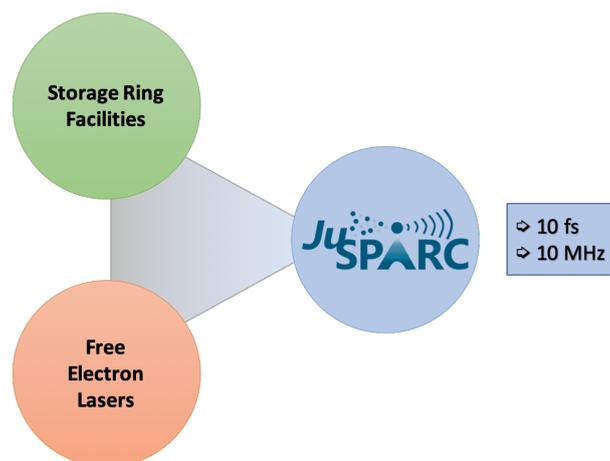


Figure 2: Positioning of *Ju*SPARC with respect to large-scale pulsed light sources.

The operation of *Ju*SPARC relies on the laser-driven production of femtosecond light pulses in a wide energy range, and the generation of ultrashort pulses of secondary particles, such as electrons. The facility comprises a set of femtosecond laser systems, which are carefully chosen with respect to pulse width, repetition rate, peak power and stability to obtain the best performance of the experiment con-

3

nected. These laser systems drive several upconversion units employing higher harmonic generation and in the future plasma wiggler schemes. The resulting XUV and x-ray pulses are monochromatized and focused into dedicated instruments for time-resolved photon and photoelectron spectroscopies and microscopies, as well as reflectivity and scattering experiments. Each experiment is also provided with phase-matched low energy photon pulses for resonant and non-resonant pumping purposes. We note that the particular modular layout of $\mathcal{J}u$SPARC will also pave the grounds for "two-colour" experiments. As an example, one could envision an experiment in which the time evolution of the crystalline and the electronic structure are investigated simultaneously by phase-synchronized probe pulses in the XUV and tender x-ray regime.

In a later stage of $\mathcal{J}u$SPARC also the acceleration and use of particle beams, such as electrons, protons and neutrons, is foreseen. While $\mathcal{J}u$SPARC's current laser systems offer too little peak intensity for an efficient particle source, they can be used for preparatory R&D studies. These will follow two pathways: (i) the acceleration of electrons in laser wake field and plasma bubble schemes for the generation of tender and hard x-ray photons, and (ii) the laser-induced acceleration of spin-polarized beams. The latter activity requires the use of pre-polarized gas targets of high density. Thus, another application of the $\mathcal{J}u$SPARC laser systems is the preparation of such targets which rely on dynamic polarization of Hydrogen atoms via the photo-dissociation of Hydrogen halides.

An overview over the current $\mathcal{J}u$SPARC laser systems is shown in Figure 3, a more detailed description can be found in the the following.
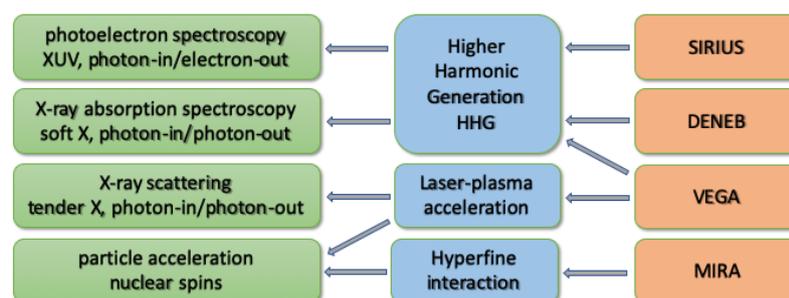


Figure 3: Assigment of the $\mathcal{J}u$SPARC laser systems (orange) to photon/spin conversion mechanisms (blue) and physics applications (green).

## 3   The Laser Systems

### 3.1   *Ju*SPARC_VEGA − Terawatt-Class Optical Amplifier

The robust, advanced, high power pulsed laser system *Ju*SPARC_VEGA (see Figure 4) has been commissioned in the beginning of 2019 and will serve for cutting-edge scientific studies of time-dependent phenomena on femtosecond time scales. This system will provide novel means to investigate ultrafast and non-linear phenomena in condensed matter-, material-, information- and energy research. A large versatility in microscopy and scattering experiments will be obtained by generating and exploiting short photon pulses in a wide range of energies from the infrared through visible up to soft X-rays. The parameters of the laser system (cf. Table 1) are first and foremost determined by the time scales of processes governing the electronic-, spin-, and structural transient states of matter.
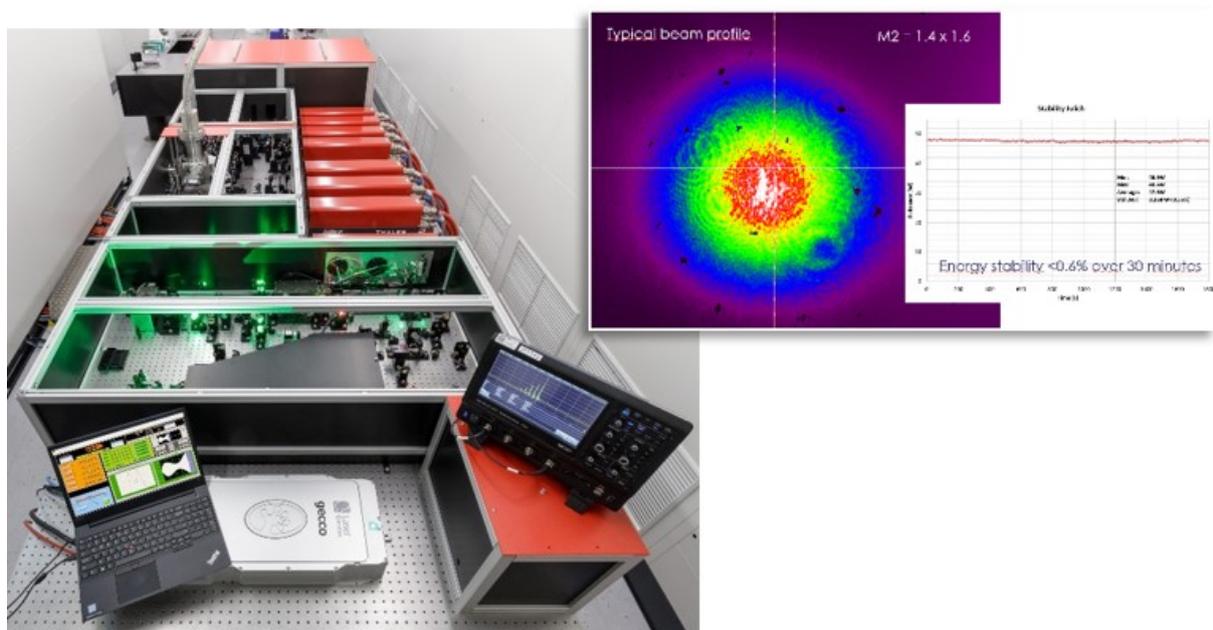


Figure 4: Overview of the 1.3 TW two-stage amplifier built by THALES, consisting of an oscillator (front), the first amplification stage (front), the second amplification stage with cryocooled Ti:Sapphire crystal (middle left), eight pump lasers (middle right, red) and the compressor unit (far side).The typical beam profile and output energy stability are shown on the right.

| Manufacturer: Thales | | | |
|---|---|---|---|
| Energy per pulse | up to 38 mJ | Peak power | 1.3 TW |
| Wavelength | 800 nm | Repetition rate | 1 kHz |
| Pulse duration | 29 fs | Average power | 38 W |
| Picosecond Contrast | $\geq 10^{-4}$ at 5 ps $\geq 10^{-5}$ at 10 ps $\geq 10^{-6}$ at 100 ps | Nanosecond Contrast | $\geq 10^{3}$ discrete pre-pulse $\geq 10^{2}$ discrete post-pulse |
| Power drift | <2% over 1h | $M^2$ | 1.8 |
| Pulse to pulse energy stability: <1% RMS over 500 shots | | | |
| Up-converted radiation: Extreme ultraviolet (EUV) light | | | |
| Experimental technique: Photon-in/photon-out, EUV detection in CCD detector | | | |

Table 1: Main output parameters of laser system for generation of high energy photons and electron acceleration.

The primary application of the *Ju*SPARC_VEGA laser system is the production of high-energy photons based on high-harmonics generation (HHG). In recent years the HHG technique has become a cutting edge experimental tool in laser spectroscopy and solid state physics using table-top laser systems. The nonlinear interaction with target-gas atoms generates frequencies at odd multiples of the driving laser. These can extend over a wide photon energy range of 10—1000 eV and retain the polarization/coherence properties and time structure of the driving laser provided that the laser pulse duration, pulse peak energy and wavelength fulfill ionization and phase matching conditions for a specific HHG medium. In the extreme ultraviolet (EUV) range (50—250 eV) pulse energies up to $\sim 10$ nJ can be achieved by using either a gas jet or a hollow wave guide geometry.

### 3.1.1   Seed laser and the first amplification stage

The first stage of *Ju*SPARC_VEGA is seeded by an oscillator built by Laser Quantum that delivers ultra-short pulses ($\geq 15$ fs) at the nJ level and 80 MHz repetition rate. The hermetically sealed oscillator is based on chirped mirror technology to deliver a broad frequency spectrum. Both the oscillator and its pump laser are operated by a single controller. After leaving the oscillator the pulse is stretched in a triplet, stretching the pulse duration to more than 150 ps (FWHM). This design ensures stretching of a large spectrum with low aberrations. It includes THALES patented technique (patent №01 16560) which better compensates for high orders of dispersion and minimizes the overall footprint (8 passes on one grating). Following the stretcher, an Acousto-Optic Programmable Dispersion Filter (AOPDF-Dazzler) is inserted into the beam path in order to allow for the independent shaping of the amplitude and pulse phase. Gain-narrowing compensation and fine tuning of the phase performed by the Dazzler lead to optimum compression.

A regenerative amplifier with a Brewster-angle cut Ti:Sa crystal operates in air and uses an innovative crystal-mount design with direct water cooling and an novel pumping geometry to assure that no stress is applied on the crystal and the coating. The Ti:Sapphire crystal, pumped by part of a Jade 2 Nd:YLF laser running at 1 kHz, amplifies the pulses to the mJ level with excellent beam profile, beam pointing and energy stability. Special care is taken to avoid pulse replicas in the picosecond domain in the regenerative cavity by using a pair of wedged polarizers associated to a single Pockels cell in the regenerative cavity to minimize dispersion. At the regenerative amplifier output, a two-pass amplifier booster stage (including a water cooled Plano/Plano Ti:Sapphire crystal) pumped by the remaining part (15 mJ) of the first Jade 2 laser brings the pulse energy up to 3.2 mJ.

After the booster, a pulse cleaner has been inserted to improve the nanoseconds contrast by two orders of magnitude. This module consists of two polarizers and a Pockels cell similar to the one used in the regen cavity. The Pockels cell driver delivers up to 8 kV voltage allowing pulse cleaning in a single pass scheme.

### 3.1.2   Pump lasers and the second amplification stage

After leaving the first amplification stage, the pulses are amplified in a 5-pass cryogenically cooled amplifier pumped by seven Jade 2 pump lasers (see Figure 5). The Brewster cut Ti:Sapphire crystal of this second stage is cooled down to 40 K (without thermal load) by a closed loop Helium circulation system. The primary circuit (compressor and cold head) is separated from the secondary circuit by a three meter long transfer line to minimize vibration transmission to the crystal. All mirrors in the multi-pass are flat to avoid any astigmatism in the beam. A lens-based imaging system is used between second and the third pass to optimize infrared pump matching and to obtain high energy extraction of $\geq 30\%$ in this amplifier.

### 3.1.3   Pulse compressor

The pulses are compressed in a Treacy type compressor operating in air. Gratings are manufactured on ZerodurTM substrate to avoid spatial distortion due to the high average power in the compressor. The
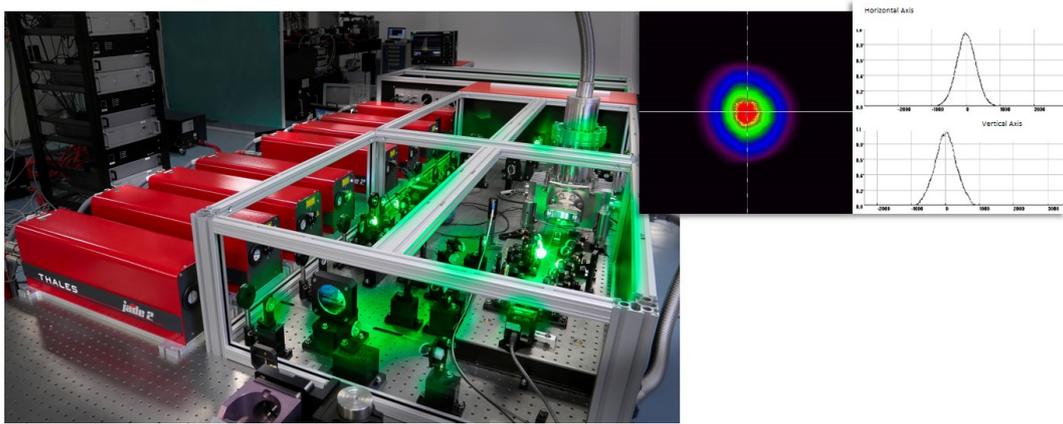
Figure 5:    The block of eight pump lasers and the second amplification stage.  The first pump laser is used to pump the first amplification stage, while the remaining seven pump lasers are employed for pumping the cryo-cooled Ti:Sapphire crystal of the second amplification stage. The typical beam profile of a Jade 2 pump laser is shown on the right.

compressor compensates the dispersion introduced by both the stretcher and the amplification stages. The beam diameter in the compressor has has been expanded in order to keep the fluence on the gratings below $10W/cm^2$ — which is considered as a safe operation design to avoid thermally induced distortion. The bandwidth of the compressor is 100 nm, fully suitable to handle 30 fs pulse compression assuming Gaussian spectrum. The pulse duration measured after the compressor is shown in Figure 6 (red curve).
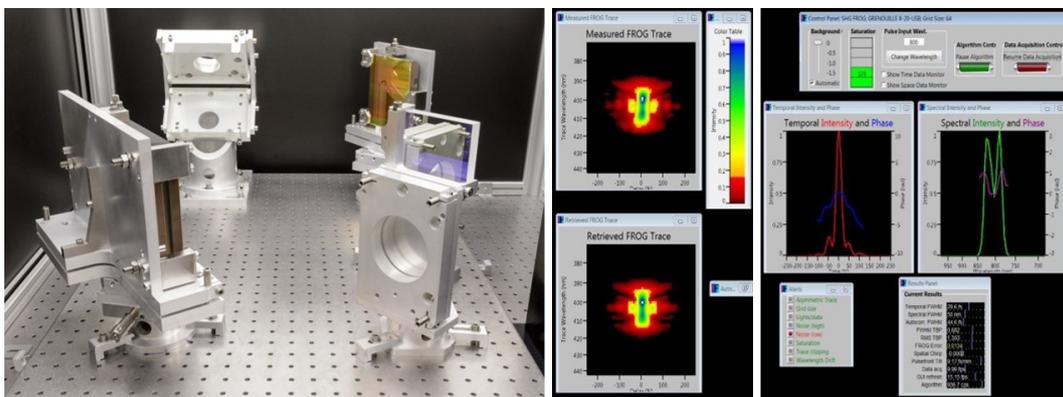


Figure 6:  Left: Compressor operating in air with Zerodur gratings aligned in Treacy configuration can compress 40 mJ input pulses.  The right panels show the measured and calculated FROG traces (left) and temporal and spatial intensity of the pulses revealing 29 fs pulse duration and 80 nm spectral width at the compressor output.

### 3.1.4  EUV Beamline

The EUV photons are generated by focusing the 29 fs short laser pulses from $\mathcal{J}u$SPARC_VEGA into a HHG source chamber (see Figure 7) using a combination of a four-inch flat mirror and an off-axis parabola with 90 mm focal length. Both mirrors are placed inside the first (focusing) chamber and the beam is then guided into the source chamber. Here it is focused to a tight spot with a size of $\sim 20\mu$m in 1/e diameter. The source itself is a metallic cell with diameters varying between 2 and 5 mm filled with a noble gas (Ar, Ne, He). After the HHG source, the generated EUV light propagates in vacuum in

7

order to avoid absorption. A mirror with a central 4 mm hole placed in the second half of the chamber separates the EUV light from the fundamental beam. At the same time the source chamber is divided in two parts by a small aperture for the passing beam to allow differential pumping of the residual gases from the source placed in the first half of the chamber. After the rejection of the infrared beam the EUV light is guided into the monochromator chamber.
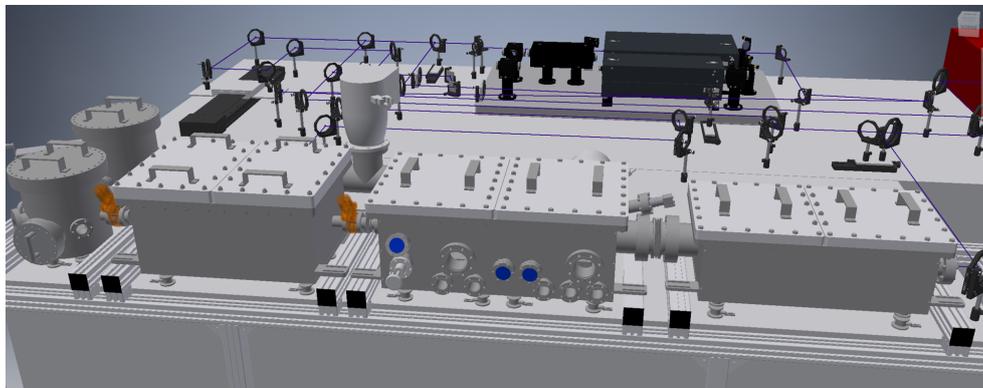


Figure 7: HHG beamline for high-energy photon and electron scattering experiments. From right to left: focusing chamber, HHG source chamber containing the gas cell, monochromator, and experiment and detection chambers. The high-energy photon beam is generated and guided inside vacuum to avoid scattering in air.

The resulting spectrum of the EUV light generated by the source has a comb-like structure consisting of odd harmonics of the driving laser. The beam approaches the sample at an angle of $45°$ with respect to the detection direction. Depending on the experimental requirements one can use one of three available beamline geometries: 1) A Bragg mirror monochromator (Gang et al., 2018) can select a narrow range of wavelengths from the entire spectrum and then probe the response of a specific element in a sample. 2) Alternatively, one can choose to focus an entire EUV spectrum onto a sample with a toroidal mirror. The entire harmonic spectrum is then focused onto the material under test and the scattered EUV light is subsequently spectraly split using reflection grating and detected by a EUV sensitive CCD camera. 3) Finally, circularly polarized EUV - available after extension of the beamline - can be employed in order to probe out-of-plane magnetized sample in transmission geometry.

The detection branches of the beamline include a McPherson spectrometer and X-ray sensitive CCD camera with up to $2024 \times 2024$ pixels. In addition an electron spectrometer with a permanent dipole magnet and phosphor screen with a high resolution CCD camera will be included after the source chamber for spectraly-resolved electron detection.

In one of our a proof of principle experiments using full spectrum T-MOKE (see Figure 8) we were able to observe spin dynamics in simple magnetic alloys and multilayers element selectively. In recent years, intensive studies of spin dynamics have been driven largely by a demand for high-speed- and high-density magnetic storage. At the same time an increasing effort has been directed towards mastering the control of the spin alignment by laser light. A number of distinct models have been proposed to describe how laser excitation can couple to the spins. Most of these models are based on phonon-, electron-, or magnon mediated spin-flip processes, direct laser-induced spin-flips or relativistic spin-light interaction. Recently, a model based on superdiffusive spin transport has been proposed. The variety of these distinct interpretations suggests that several physical mechanisms may govern femtosecond spin-dynamics even in a simple elemental magnet. The analysis becomes even more complex for heterogeneous magnetic systems, such as magnetic alloys and exchange-coupled layered structures. The detailed understanding of spin dynamics in complex magnetic alloys and multilayers requires testing of the electronic and magnetic properties element-selectively with femtosecond time resolution, at the same time. Element selective studies of complex alloys and materials have been addressed for some
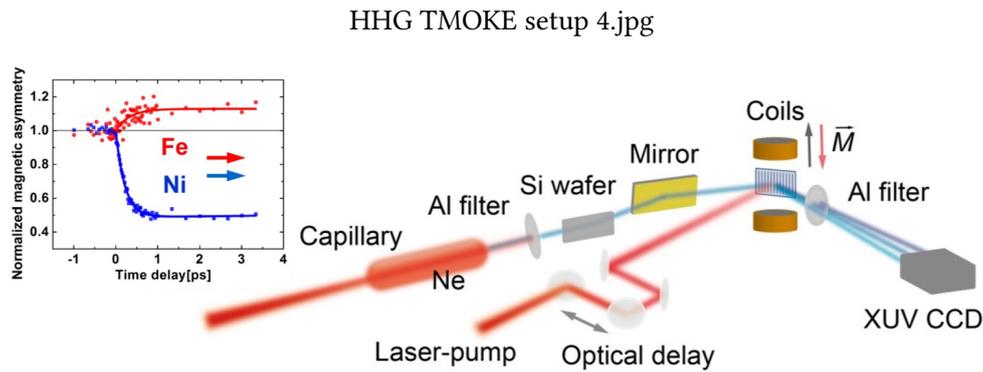
HHG TMOKE setup 4.jpg



Figure 8: Experimental setup for element-selective spin dynamics. The laser pump and XUV probe beams are derived from a single laser amplifier. The XUV light propagates in vacuum and contains a spectrum of photons with energies between 20 and 72 eV. The inset (left) shows time-resolved magnetization of the Fe and Ni layers in the Fe/Ru/Ni trilayer. The magnetic asymmetry at the Fe 3p absorption edge anomalously increases for the parallel magnetic orientation of Ni and Fe layers thus confirming the presence of laser-driven spin superdiffusion from Ni to Fe layer.

time using synchrotron radiation by tuning the light to the characteristic resonances of a particular material. In our studies we used similar approach but in addition, we employed a laser-based XUV light sources generating femtosecond pulses with photon energies reaching up to 72 eV. By exploiting the transversal magneto-optical Kerr effect near the M absorption edges of nickel (66.5eV) and iron (52 eV) we obtained magnetic contrast as large as 20% for Ni and 10% for Fe near the Brewster angle of about 45 degrees. Combining element selectivity with femtosecond time resolution we studied the magnetic response of ferromagnetic Ni(5nm)/Ru(1.5nm)/ Fe(4nm) multilayers. By exciting the multilayer with infrared laser light we observed the evolution of magnetization response in the Ni and Fe layers simultaneously but separately using synchronized XUV probe pulses detecting spin response within 3.5ps after laser excitation (see inset (left) in Figure 8). Following the excitation, we detected an unexpected fluence-dependent magnetization enhancement in the buried Fe layer for parallel alignment of Fe and Ni magnetization. The experiments confirmed the existence of optically generated superdiffusive spin currents experimentally for the first time. The follow-up experiments using $\mathcal{J}u$SPARC_VEGA are expected to broaden the range of the materials accessible by this advanced technique. In the long term perspective even more advanced excitation- and probe-beams, including THz, IR, soft X-rays or even monochromatic electron beams will be available. These emerging capabilities will allow a detailed insight and precise control of electronic processes in modern quantum materials on ultrafast time-scales.

### 3.2 *Ju*SPARC_DENEB

Being commissioned in 2010 *Ju*SPARC_DENEB (cf. Figure 9 and Table 2) has been the first laser-based
EUV source at the Peter Grünberg Institute. The experiments performed with *Ju*SPARC_DENEB con-
tributed substantially to the understanding processes governing the spin dynamics in magnetic mate-
rials. In addition, the experiments served to develop tools for EUV detection, experimental procedures
and methodology, as well as to specify physical questions requiring an ultrafast EUV source such as
the *Ju*SPARC_VEGA system described above.

Progress in magnetic information storage and processing technology is intimately associated with com-
plex materials that are engineered at the nanometer scale. Next-generation devices require that the
magnetic state of materials can be manipulated on fast timescales and at the nanometer level. The fun-
damental question of whether the magnetization dynamics of individual elements in a ferromagnetic
alloy can differ on ultrafast timescales is very important and have been addressed either theoretically
or experimentally in only extremely limitted number of studies.

One way to experimentally answer this question is to excite a complex sample by successive ultrashort
($\sim$ 35 fs) laser pulses and probe the demagnetization dynamics with EUV pulses that allow one to
explore the involved spin dynamics element-specifically.



Figure 9: Multi-pass laser amplifier (KMLabs) providing 2 mJ pulse energy at 3 kHz forms the core
of the *Ju*SPARC_DENEB laser system commissioned for spin dynamics experiments in thin magnetic
films and multilayers.

| Manufacturer: | KMLabs |
|---|---|
| Repetition rate | 3 kHz |
| Pulse duration | 35 fs |
| Pulse energy | 2.2 mJ |
| Average power | 6.6 W |
| Up-converted Radiation | Extreme UV light |
| Conversion principle | High harmonics generation (HHG) |
| Experimental technique | Photon-in / photon-out<br>Detection of scattered XUV photons in CCD detector |

Table 2: Main parameters of *Ju*SPARC_DENEB.

In 𝒥𝑢SPARC_DENEB sub-10 fs XUV light pulses are provided by the HHG process, after focusing 2.2 mJ femtosecond IR laser pulses into a Ne-filled glass wave guide. The generated harmonic photon energies of 35–72 eV cover the M absorption edges of the ferromagnetic elements Fe (54 eV) and Ni (67 eV) and Co (60 eV). The optical-pump – EUV-probe experiments provide information on open questions in femtosecond magnetization dynamics in the case of metallic, multi-species, exchange-coupled systems (La-O-Vorakiat et al., 2012; Mathias et al., 2012; Rudolf et al., 2012).

Over the last years, the driving mechanism of laser-induced demagnetization has been intensively studied in systems such as magnetic tri-layers and thin films showing magnetic domain structures. Among several proposed mechanisms responsible for ultrafast demagnetization, in these structures is the significant contribution of super-diffusive spin currents. The comparison of both the perpendicular spin diffusion into adjacent layers and the lateral diffusion along the sample plane requires well defined magnetic structures and sophisticated measurement techniques. For instance, the lateral spin diffusion has been associated with a softening of the domain walls. Such surveys demand a photon-based imaging experiment with a sufficient spatial sensitivity, which is provided by resonant magnetic scattering (RMS). This technique allows unique investigations of magnetic domains due to several reasons. First, it is element selective, in contrast to magnetic force microscopy (MFM), and it can resolve magnetic structures in the reciprocal space within the resolution defined by the wavelength of the radiation (1—2 nm). Second, external magnetic fields can be applied during the measurements, in contrast to electron-based imaging techniques. Finally, RMS is very sensitive to changes of the average domain arrangement, which can be difficult to track using real-space microscopes with a limited field of view. We used this powerful technique to study magnetic domains in FePd/CoPd bi-layers at a synchrotron and CoPt multi-layers using the 𝒥𝑢SPARC_DENEB laser system. Such ferromagnetic hetero-structures are very promising candidates for time-resolved and element-specific RMS experiments, using high harmonic generation source with high EUV brilliance such as 𝒥𝑢SPARC_VEGA to investigate the processes contributing to ultrafast demagnetization.

### 3.3 *Ju*SPARC_SIRIUS — Spin- and time-resolved electron dynamics

In order to give detailed information on different microscopic mechanisms governing ultrafast electron spin dynamics in magnetism and spintronics, a wavevector, spin and time resolved analysis of the electronic structure is mandatory. Utilizing the novel light source of *Ju*SPARC_SIRIUS, this task will be solved by a cutting-edge and very recently developed instrument — spin- and time-resolved electron momentum microscopy (SPEMM). Thanks to its groundbreaking multidimensional – i.e., wavevector-, spatial-, energy-, and spin-resolved – detection scheme, the SPEMM provides currently the most efficient approach to map the time-evolution of electronic states in magnetic and non-magnetic quantum materials.

#### 3.3.1 Laser system and XUV photon generation

Time resolved pump-probe measurements involve repeating the photoemission measurement many times while adjusting the variable delay between the pump- and probe-photon pulses in steps of a few femtoseconds. Consequently, the collection of individual band structure dispersions, Fermi surface maps, or photoemission electron microscopy (PEEM) images requires a high measurement efficiency. In most existing high harmonic generation (HHG) setups, however, a low repetition rate (usually well below 1 MHz) and a large number of photons per pulse poses a fundamental limitation to this measurement efficiency. The reason is that, as in all photon-in-electron-out based techniques, Coulomb repulsion within the electron ensemble sets a fundamental limit for the maximum number of electrons that can be emitted by one photon pulse. As a consequence, with a limited photoelectron flux at typical kHz repetition rates the acquisition of multidimensional photoelectron spectra requires impractically long acquisition times. Besides the technological challenges imposed by, e.g., laser instabilities, extended acquisition times are prohibitive for many experiments due to aging effects and sample degradation. While the interaction of an electron with the average charge distribution of all other electrons (space–charge interaction) is a deterministic process that can be partly corrected in a momentum microscope, individual e–e processes lead to an irreversible broadening of the ensemble and thus distortions of the observables, i.e., momentum, position, or kinetic energy. These space–charge effects may be avoided by increasing the repetition rate, instead the intensity of a single photon pulse. In the ideal case, a number of 1–10 electrons per XUV photon pulse at maximum are emitted from the sample within a time of 100 fs. Under these conditions, the space–charge effect becomes negligible, and the efficiency of the measurement increases linearly with the photon pulse repetition rate. Above consideration clearly shows that the XUV light source for time-resolved photoemission experiments demands for high repetition rates in the multi-MHz regime.
Time-resolved photoemission experiments have been for a long time limited in the pump (1.5 eV) and probe (6 eV) energies available. Tabletop HHG light source represents a coherent version of the Röntgen X-ray tube, with fs pulse duration and unprecedented spectral coverage of 1-100 nm, making it ideal to capture the fastest process in 2D and 3D materials. HHG is based on up-conversion of infrared photons into XUV photons through the highly nonlinear interaction of an intense laser pulse with gas molecules. To achieve a sufficient output of coherent XUV photons, a high average power and a short pulse duration of the infrared laser systems are required. The HHG with repetition rates up to 4 MHz and a photon energy up to 40 eV was recently successfully demonstrated using ultrashort laser pulses in a conventional gas jet target (Chiang et al., 2012). However, to date state-of-the-art HHG sources with a combination of high photon energies and high repetition rates still remain an open challenge.
Figure 10 shows the principle of *Ju*SPARC_SIRIUS combined with the recent newly developed high-power ultrafast laser system that exploits the novel inventions of the innoslab fs-amplifier (Russbueldt et al., 2015) and nonlinear pulse compression (Weitenberg et al., 2017) to accomplish ultrashort laser pulses (100 fs), large average-power (500 W), and a high repetition-rate (10 MHz). The main parameters of the *Ju*SPARC_SIRIUS laser system are listed in Table 3. This high-power laser is placed in a localized clean room established by multi-stage air filter systems with a low-turbulence and laminar airflow to
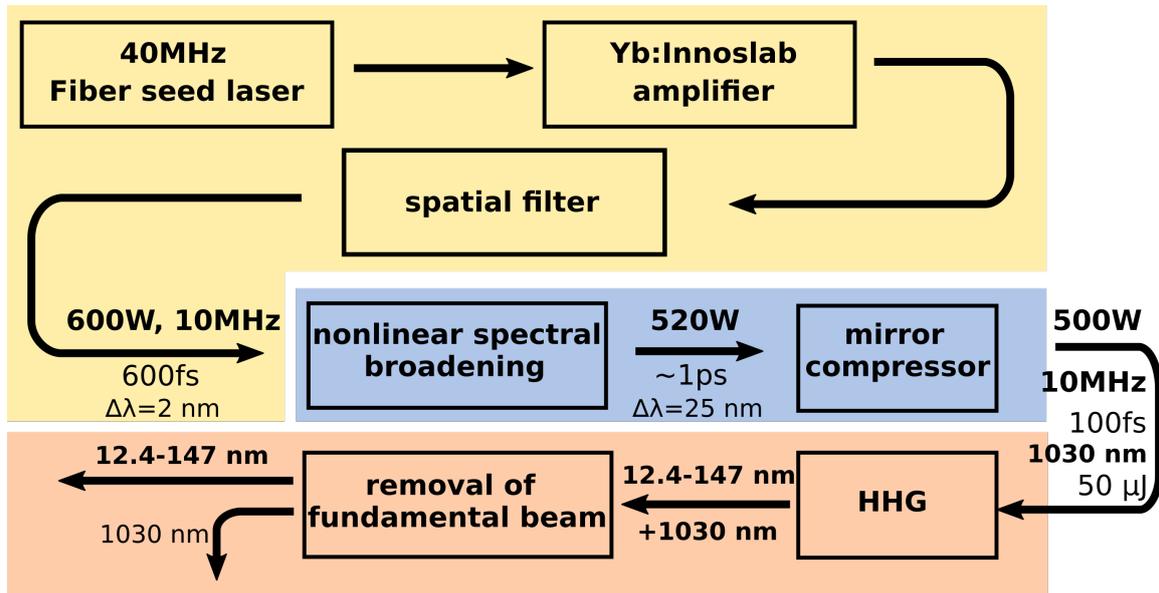
Figure 10: Schematic setup of $\mathcal{J}u$SPARC_SIRIUS for spin- and time-resolved electron momentum microscopy, which consist of Innoslab amplifier (shaded yellow region) (Russbueldt et al., 2015), nonlinear compression using multi-pass cell (Weitenberg et al., 2017) (shaded blue region) and XUV-initiated HHG (shaded orange region).

| Manufacturer: | AMPHOS |
|---|---|
| Repetition rate | up to 10 MHz |
| Pulse duration | 100 fs |
| Pulse energy | up to 50 $\mu$J |
| Average power | 500 W |
| Up-converted Radiation | Extreme UV light |
| Conversion principle | Higher-harmonics generation (HHG) |
| Experimental technique | Photon-in / electron-out (spin-resolved detection of photoelectrons) |

Table 3: Main parameters of $\mathcal{J}u$SPARC_SIRIUS

create a particle-free environment, as shown in Figure 11.

This advanced laser system will make it possible to push towards XUV photon energies exceeding 100 eV. The new setup will provide a tabletop ultrashort-pulse light source at a multi-megahertz repetition rate to perform time-resolved momentum-microscopy measurements that capture the ultrafast dynamics of spin-polarized electronic states of novel quantum materials within the complete Brillouin.



Figure 11: Photo of 𝒥uSPARC_SIRIUS laser system. The high-power laser is operated under clean room conditions with multi-stage air filter systems, producing a low-turbulence laminar airflow to a create particle-free environment.

### 3.3.2   Beamline

In order to make use of the XUV light produced in the HHG process for photoemission, it has to be monochromatized and transported to the momentum microscope. This is solved by a line of mirrors and a grating monochromator. The overall layout is depicted in Figure 12. The XUV light generated in the gas cell is picked up by a toroidal mirror, which forms an intermediate image of the source in front of the monochromator entrance. T2 is used to collimate the light and illuminate a reflective plane grating. After diffraction at the grating, the light is focused by T3 into the exit plane, where a slit defines the energy resolution. For the use of the fs XUV pulses in time resolving experiments, we make use of a special monochromator geometry to minimize pulse broadening effects (Fabio Frassetto & Poletto, 2014). Passing through a grating monochromator affects the pulse length in two ways: (1) the monochromator acts as a frequency bandpass with a finite bandwidth. Since time and frequency are connected via Fourier transform, limiting the energy bandwidth will broaden the time profile. (2) the diffraction at a grating adds a geometric broadening of the pulse time profile due to different optical pathlenths. We adopt the design described in (Fabio Frassetto & Poletto, 2014) as off-plane-mounting, which minimizes the second effect by orienting the gratings grooves along the light incidence direction. To minimize the first effect, we design the monochromator to have an energy resolution that is just sufficient to separate adjacent harmonic lines. For experiments demanding a better definition of photon energy, the resolution of the monochromator can be increased by changing to gratings with a higher groove density and closing the exit slit. For this purpose, the monochromator will feature a grating exchange mechanic and an adjustable exit slit.
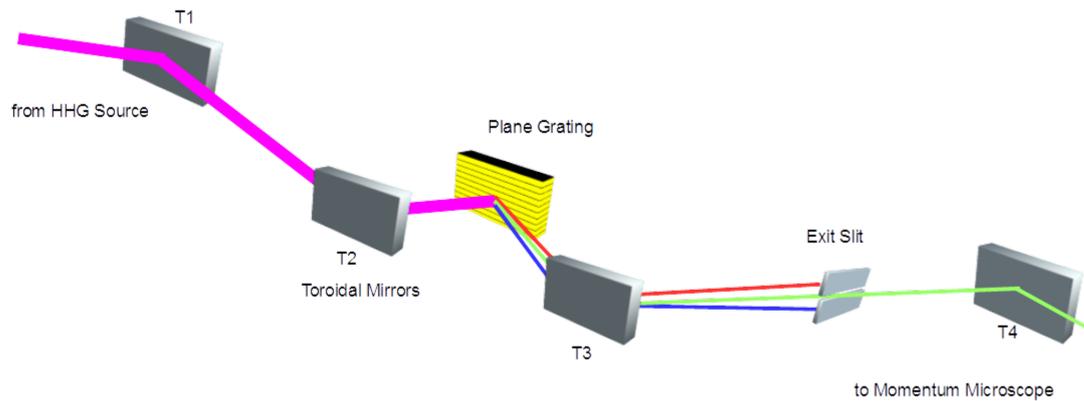
Figure 12: *Ju*SPARC_SIRIUS beamline. The XUV light, produced in the HHG process for photoemission, is monochromatized and transported to the momentum microscope.

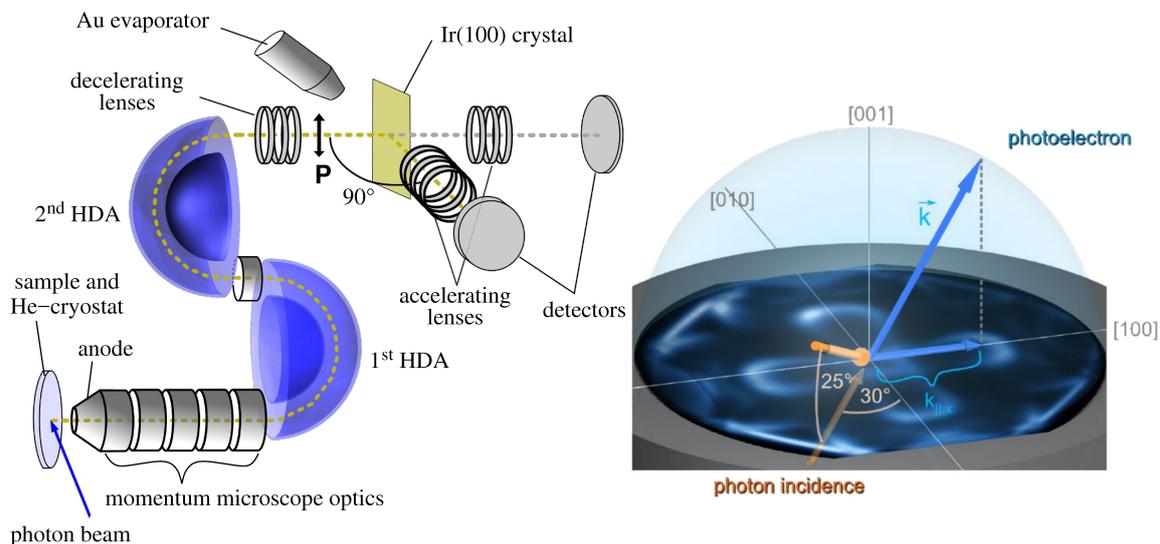### 3.3.3   Momentum microscopy facility



Figure 13: *Left side*: Working principle of a spin-resolving electron momentum microscope (SPEMM) consisting of the imaging electron optics, electrostatic energy filter, imaging spin-filter with Ir(100) mirror, and detectors (Tusche et al., 2015). *Right side*: Emission of photoelectrons into the complete half-space above the sample surface and the related intensity distribution in reciprocal space. The SPEMM experiment collects all photoelectrons simultaneously.

A momentum microscope (see Figure 13 left side) combines the concepts of high resolution photo-electron spectroscopy and photoemission electron microscopy to directly record the two-dimensional distribution of all photoelectrons excited from the sample as an image of their respective crystal momenta. The simultaneous acquisition of a large volume in reciprocal space – a cut through the Fermi surface of the investigated material is provided in a single measurement – turned out to be an extremely efficient measurement scheme for complete sets of electronic band dispersions at all points in reciprocal space.

As a single measured image, unlike as in conventional ARPES, represents directly the map of all photo-electrons as a function of their parallel momentum component ($k_x$, $k_y$) at a given energy (see Figure 13 right side), no issues due to normalization or symmetrization arise. In particular, the fixed photoemission geometry gives further direct access to symmetry dependent effects and dichroism. The simul-

taneous momentum mapping is therefore ideally suited to observe the dynamics of electrons in the Fermi-surface of a material, e.g., upon the the excitation by an ultra short pump pulse from the laser source, probed as a function of time by a second ultrashort VUV photon pulse at a given time delay. Being based on the imaging optics of an electron microscope, the SPEMM instrument is also used for the spatial imaging of the sample surface. In addition to a conventional PEEM, the electrostatic energy analyzer of the setup provides spectroscopic imaging capabilities. For instance, shallow core levels like the 3p states of the transition metals in a binding energy range of 50–60 eV can be exited already in the VUV photon energy range, providing element selectivity in time resolved PEEM experiments.

A laser based source is, in principle, very well suited to study the electronic band structure of inhomogeneous samples or nano structures, as a laser beam can be easily focused to spot sizes of about 10 $\mu$m. In the VUV range, however, further focusing into the < 1 $\mu$m regime becomes demanding due to the required use of mirror elements or zone plates. The latter approach is done nowadays at a couple of $\mu$-ARPES end stations at synchrotron radiation facilities, adding considerable complexity to the experiment. As the SPEMM is based on the electron optical imaging concepts of PEEM, such tight focusing of the excitation beam is not necessary. Instead, spatial resolution of the band structure becomes possible by selection of imaged area by the microscope. In this way, local photoelectron momentum distributions can be collected from areas down to 100 nm.

### 3.3.4   Imaging electron spin filter

A key aspect of the SPEMM facility is the imaging spin-filter technique which was recently established (Tusche et al., 2011). This approach, integrated into the momentum microscope, constitutes a major breakthrough defeating the notoriously low efficiency of electron spin polarimeters that has limited their use in spectroscopy since the 1960's. The novel concept of multichannel spin polarization analysis provides a stunning increase in spin-detection efficiency by four orders of magnitude in comparison to the performance of state-of-the-art single-channel electron spin detectors. This makes the imaging spin filter a key component of the SPEMM, as the low efficiency of conventional detectors is prohibitive for time resolved measurement of electron dynamics in the band structure or Fermi surface, or microscopic imaging.

Here, spin-filtering is based on the diffraction of low energy electrons in the (00)-LEED beam of a single crystal, acting as an spin-selective mirror. Spin contrast is obtained due to the spin-dependent reflectivity of low energy electrons, while the image information is conserved in the outgoing elastic (00) diffraction spot. It was show that several 1000 image points of a momentum image or a PEEM image can be recorded simultaneously.

Combining an ultrashort-pulse high-repetition-rate laser driven X-ray source with the highly efficient spin-resolved momentum microscope, $\mathcal{J}u$SPARC_SIRIUS will be one of the first facilities where the ultrafast dynamics of electronic states within the whole three-dimensional Brillouin zone can be studied by time-, spin- and momentum-resolved photoemission experiments.

### 3.4  *Ju*SPARC_MIRA — Control of Nuclear Spins

The generation of polarized particle beams is still relies on the use of conventional particle accelerators, which are commonly very large in scale and budget. New concepts based on laser-driven particle acceleration have initiated a large international effort in this research field. Despite much progress in understanding fundamental physical phenomena, it is largely unexplored how the particle spins are influenced by the huge magnetic fields inherently present in the plasma and, thus, how highly polarized particle beams can be produced in laser-driven plasmas.

For the experimental realization of an innovative laser-driven plasma accelerator for polarized proton beams, a novel laser-based target system is needed: two laser beams are focused into a gas jet made of bi-atomic linear molecules with at least one Hydrogen atom like, for example, HCl gas (Büscher et al., 2019; Hützen et al., 2019). The peculiarity of the used *EKSPLA SL330 series Ju*SPARC_MIRA system is the simultaneous output of the fundamental wavelength at 1064 nm and the fifth harmonic at 213 nm provided by a Nd:YAG crystal serving as active medium. Operating at a repetition rate of 5 Hz, a pulse duration of 170 ps, and a pulse energy of 100 mJ the linear polarized fundamental beam is focused onto the gas jet. By this, the molecular electric dipole moment $\mu$ is aligned relative to the electric field of the laser light leading to an increased polarization signal. Simultaneously, but under an angle of $90°$, the strongly focused circularly polarized fifth harmonic beam with an intensity of $\sim 10^{12}\,\mathrm{Wcm^{-2}}$ is also guided into the vacuum chamber. The interaction with the already aligned HCl molecules leads to a photo-dissociation process by UV excitation and, finally, the polarization of the H nuclei via hyperfine spin beating. The polarization of the atomic hydrogen ensemble can be optimized with a Lamb-Shift polarimeter (Engels et al., 2005, 2003).

For guiding the fifth harmonic beam, customized optics with a diameter of one inch for a beam diameter of 12 mm are used. The most important requirement for the mirrors is the highest possible light reflectance which is realized by a optical coating technology, the so-called ion beam sputtering. This technique is provided by *LAYERTEC GmbH* and promises a very strong climate and mechanical stability, a high coating accuracy as well as very little light scattering (reflectively > 98 % at $45°$ incidence angle). For converting the initially linearly polarized laser beam to circular polarization a quartz quarter-wave plate with two-sided anti-reflection coating from *EKSMA Optics* is used. A plano-convex lens finally focuses the UV beam slightly below the HCl outlet nozzle inside the vacuum interaction chamber. The fundamental beam at 1064 nm is guided by standard mirrors with dielectric Nd:YAG coatings offering high reflectivity for p- and s-polarized light and providing high damage thresholds. A 150 mm long linear translation stage is integrated in the beam path to spatially overlap the two laser beams in the interaction point just below the gas nozzle. In order to focus the fundamental wavelength to an intensity of $\sim 5 \cdot 10^{13}\,\mathrm{Wcm^{-2}}$ into the HCl gas first the beam is expanded by two lenses aligned in reverse Galilean arrangement and thus directed to two further lenses right in front of the interaction chamber. A photo-diode, exchangeable with the gas nozzle, guarantees the control of the spatial and temporal overlap of the two beams.

| Manufacturer: | EKSPLA |
|---|---|
| Repetition rate | 5 Hz |
| Pulse duration | 170 ps |
| Pulse energy | 100 mJ @1064 nm, 20 mJ @213 nm |
| Average power | 0.5 W |
| Up-converted Radiation | 532 nm, 266 nm, 213 nm |
| Conversion principle | Built-in 2nd to 5th harmonic generator |
| Experimental technique | Control of nuclear spins via photo-dissociation |

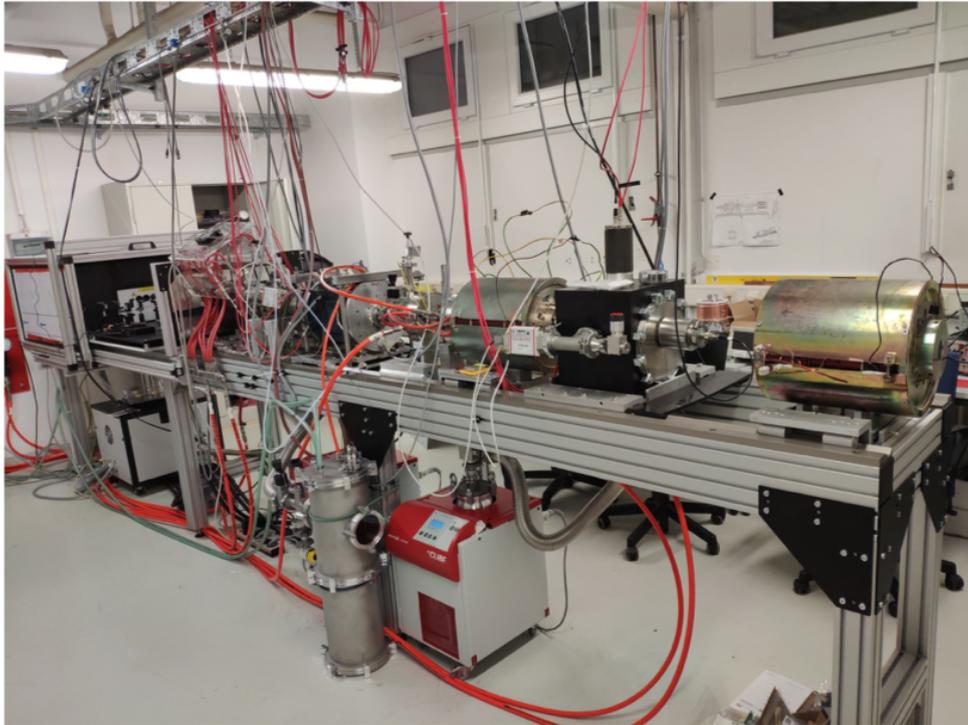Table 4: Main parameters of *Ju*SPARC_MIRA

Figure 14: Photo of $\mathcal{J}u$SPARC_MIRA and the Lamb-shift polarimeter.

The ultimate goal of building the next generation of highly compact and cost-effective electron and proton accelerator facilities using a plasma as the accelerating medium requires three challenges to be meet:

(i) alignment of the electron/proton spins before accelerating laser irradiation since a significant build-up of the polarization, unlike at conventional accelerators, cannot happen in an initially unpolarized target (Büscher et al., 2019; Hützen et al., 2019; Thomas et al., 2019). On the other hand, an initially polarized particle ensemble can be depolarized via spin precession around the laser or plasma magnetic fields This effect is characterized by the Thomas-Bargmann-Michel-Telegdi (T-BMT) equation.

(ii) Injection and related polarization losses of low energetic ($\gamma \approx 1$) particles in the laser- or wake-field have be to controlled and minimized. For electrons Wu et al. recently proposed a new concept based on vortex Laguerre-Gaussian (LG) laser-driven wake-field acceleration (Wu, Ji, Geng, abd Neng-wen Wang, et al., 2019; Wu, Ji, Geng, Yu, et al., 2019). Using the target technology described above with the $\mathcal{J}u$SPARC_MIRA laser system and then shooting the vortex LG laser pulse, full three-dimensional particle-in-cell simulations promise the preservation of the electron spin polarization according to T-BMT equation by more than 80 %. Furthermore, compared to Gaussian beams, with this technique efficient injection and a boost in the peak flux of more than one order of magnitude is guaranteed.

(iii) Steady acceleration of already relativistic ($\gamma \gg 1$) particles in the laser wake-field must be ensured. Thomas et al. show that a perturbation of the single-particle trajectories is influenced rather by T-BMT rotation-induced spin changes than due to a coupling of the spin to the energy- or velocity-changing rates for the generalized Stern-Gerlach force in the case of high-energetic ($\gamma \gg 1$) and weakly relativistic ($\gamma \approx 1$) particles (Thomas et al., 2019). For GeV protons the minimum polarization time is in the order of microseconds corresponding to a particle-field interaction time is in the nanosecond range. Estimations of the particle depolarization time based on the T-BMT equation indicate duration in the range of picoseconds. Hence, polarization conservation during the interaction with passing picosecond laser pulse is guaranteed.

# References

Büscher, M., Hützen, A., Engin, I., Thomas, J., Pukhov, A., Engels, R., … Sofikitis, D. (2019). Polarized proton beams from a laser-plasma accelerators. *Int. J. Mod. Phys. A*, *34*, 1942028. http://dx.doi.org/10.1142/S0217751X19420284

Chiang, C.-T., Blättermann, A., Huth, M., Kirschner, J., & Widdra, W. (2012). High-order harmonic generation at 4 mhz as a light source for time-of-flight photoemission spectroscopy. *Appl. Phys. Lett.*, *101*(7), 071116. http://dx.doi.org/10.1063/1.4746264

Engels, R., Emmerich, R., Grigoryev, K., Paetz gen. Schieck, H., Ley, J., Mikirtytchiants, M., … Vassiliev, A. (2005). Background reduction by a getter pump around the ionization volume of a Lamb-shift polarimeter and possible improvements of polarized ion sources. *Rev. Sc. Instrum.*, *76*, 053305. http://dx.doi.org/10.1063/1.1898923

Engels, R., Emmerich, R., Ley, J., Tenckhoff, G., Paetz gen. Schieck, H., Mikirtytchiants, M., … Vassiliev, A. (2003). Precision Lamb-shift polarimeter for polarized atomic and ion beams. *Rev. Sc. Instrum.*, *74*, 4607. http://dx.doi.org/10.1063/1.1619550

Fabio Frassetto, P. M., & Poletto, L. (2014). Grating configurations for the spectral selection of coherent ultrashort pulses in the extreme-ultraviolet. *Photonics*, *1*, 442 - 454. http://dx.doi.org/10.3390/photonics1040442

Gang, S.-g., Adam, R., Plötzing, M., von Witzleben, M., Weier, C., Parlak, U., … Oppeneer, P. M. (2018, Feb). Element-selective investigation of femtosecond spin dynamics in nipd magnetic alloys using extreme ultraviolet radiation. *Phys. Rev. B*, *97*, 064412. http://dx.doi.org/10.1103/PhysRevB.97.064412

Hützen, A., Thomas, J., Böker, J., Engels, R., Gebel, R., Lehrach, A., … Büscher, M. (2019). Polarized proton beams from laser-induced plasmas. *High Power Laser Science and Engineering*, *7*, e16. http://dx.doi.org/10.1017/hpl.2018.73

Ielmini, D., & Waser, R. (2016). *Resistive switching: From fundamentals of nanoionic redox processes to memristive device applications* [Edited Book]. Wiley.

La-O-Vorakiat, C., Turgut, E., Teale, C., Kapteyn, H., Murnane, M., Mathias, S., … Silva, T. (2012). Ultrafast demagnetization measurements using extreme ultraviolet light: Comparison of electronic and magnetic contributions. *Phys. Rev. X*, *2*, 011005. http://dx.doi.org/10.1103/PhysRevX.2.011005

Mathias, S., La-O-Vorakiat, C., Grychtol, P., Granitzka, P., Turgut, E., Shaw, J., … Kapteyn, H. P. (2012). Probing the timescale of the exchange interaction in a ferromagnetic alloy. *Proc. Natl. Acad. Sci.*, *109*, 4792. http://dx.doi.org/10.1073/pnas.1201371109

Rudolf, D., La-O-Vorakiat, C., Battiato, M., Adam, R., Shaw, J. M., Turgut, E., … Oppeneer, P. (2012). Ultrafast magnetization enhancement in metallic multilayers driven by superdiffusive spin current. *Nat. Comm.*, *3*, 1037. http://dx.doi.org/10.1038/ncomms2029.

Russbueldt, P., Hoffmann, D., Höfer, M., Löhring, J., Luttmann, J., Meissner, A., … Poprawe, R. (2015). Innoslab amplifiers. *IEEE J. Sel. Top. Quantum Electron.*, *21*(1), 447-463. http://dx.doi.org/10.1109/JSTQE.2014.2333234

Thomas, J., Hützen, A., Lehrach, A., Pukhov, A., Liangliang, L., Wu, Y., & Büscher, M. (2019). Scaling laws for the (de-)polarization time of relativistic particle beams in strong fields. *Publication in preparation for Phys. Rev. Accel. Beams.*

Tsymbal, E., & Zutic, I. (2012). *Spin transport and magnetism* [Book]. Boca Raton: CRC Press.

Tusche, C., Ellguth, M., Ünal, A. A., Chiang, C.-T., Winkelmann, A., Krasyuk, A., . . . Kirschner, J. (2011). Spin resolved photoelectron microscopy using a two-dimensional spin-polarizing electron mirror. *Appl. Phys. Lett.*, *99*(3), 032505. http://dx.doi.org/10.1063/1.3611648

Tusche, C., Krasyuk, A., & Kirschner, J. (2015). Spin resolved bandstructure imaging with a high resolution momentum microscope. *Ultramicroscopy*, *159*, 520 - 529. (Special Issue: LEEM-PEEM 9) http://dx.doi.org/https://doi.org/10.1016/j.ultramic.2015.03.020

Weitenberg, J., Vernaleken, A., Schulte, J., Ozawa, A., Sartorius, T., Pervak, V., . . . Hänsch, T. W. (2017). Multi-pass-cell-based nonlinear pulse compression to 115 fs at 7.5 $\mu$j pulse energy and 300 w average power. *Opt. Express*, *25*(17), 20502–20510. http://dx.doi.org/10.1364/OE.25.020502

Wu, Y., Ji, L., Geng, X., abd Nengwen Wang, Q. Y., Feng, B., Guo, Z., . . . Li, R. (2019). Polarized electron-beam acceleration driven by vortex laser pulses. *New J. Phys.*, *21*(7), 073052. http://dx.doi.org/10.1088/1367-2630/ab2fd7

Wu, Y., Ji, L., Geng, X., Yu, Q., Wang, N., Feng, B., . . . Li, R. (2019). Polarized electron beam generation in plasma-driven wakefield acceleration. *Phys. Rev. E*, *100*, 043202. http://dx.doi.org/10.1103/PhysRevE.100.043202